3-Dimensional Methylammonium and Ammonium Templated Lithiumberyllofluoro Frameworks

Lee A. Gerrard and Mark T. Weller*

School of Chemistry, University of Southampton, Highfield, Southampton, Hants S017 1BJ, U.K.

Received December 12, 2003. Revised Manuscript Received February 6, 2004

Two three-dimensional lithiumberyllofluoride materials, of the same framework stoichiometry but different topologies, have been synthesized using hydrothermal pressure conditions and ammonium/methylammonium cations as structure-directing species. Compound **I**, $[Li_2Be_2F_7][NH_4]$, and compound **II**, $[Li_2Be_2F_7][CH_3NH_3]$, both crystallize in orthorhombic space groups: $Pca2_1$ for **I** and *Cmcm* for **II**. Single crystal analysis reveals that the materials have slightly different 3-D framework topologies for the $[Li_2Be_2F_7]$ framework composed of $[LiF_4]$ and $[BeF_4]$ tetrahedra connected through doubly and triply bridging fluorides. Both networks can be viewed as sheets formed of 3- and 4-nets that link perpendicular to the sheet, through a bridging fluoride, to form six-membered interlayer pores. The six-membered channels contain the amine species hydrogen-bonded to framework fluoride ions surrounding the interior of the pore. The thermal stability, spectroscopic properties, and both powder X-ray and neutron data of these compounds are reported, along with the single-crystal analysis used to solve the structures.

Introduction

Microporous, zeotype materials are currently of great interest because of their diverse properties of catalytic,[1] ion exchange selectivity,[2] and electronic/magnetic[3] behaviors. At present the main focus of the synthesis of these materials lies with forming both new framework topologies and new chemical compositions. The majority of materials in this class are metal-oxide frameworks, as in zeolites,[4] aluminophosphates,[5] and some transition metal phosphates.[6] Recently, other oxide-based materials using 4, 5, and 6-coordinate cationic species, such as V(IV/V),[7] Ga(III),[8] Co(II),[9] and Zn(II),[10] have been studied because of the inherent structural diversity derived from using the different metallic coordination geometries. Formation of these frameworks usually requires the presence of a specific templating species to direct the adoption of a particular structural topology. For example, a plethora of 3-D neutral framework (solely AlO_4/PO_4) and anionic framework (AlO_4, AlO_5, AlO_6/PO_4, $PO_3(=O)$, $PO_3(OH)$, as well as others) aluminophosphate-based materials have been synthesized using organoamine structure-directing agents.[11−16]

Instead of varying either the template or the cationic framework species, altering the anionic linking species, i.e., O^{2-} for F^-, may afford new structure types. Framework topologies constructed from $[MF_4]$ tetrahedral building units are known but are very uncommon.[17,18]

* To whom correspondence should be addressed. E-mail: mtw@soton.ac.uk. Fax: (+44) 23 80 59 3781. Tel: (+44) 23 80 59 3592.

(1) (a) Corma, A.; Rey, F.; Valencia, S.; Jorda, J. L.; Rius, J. *Nat. Mater.* **2003**, *2*, 493−497. (b) Corma, A.; Diaz-Cabanas, M.; Martinez-Triguero, J.; Rey, F.; Rius, J. *Nature* **2002**, 418, 514−517. (c) Long, R. Q.; Yang, R. T. *J. Am. Chem. Soc.* **1999**, *121*, 5595−5596. (d) Thomas, J. M. *Angew. Chem., Int. Ed. Engl.* **1994**, *33*, 913−937.

(2) (a) Bhaumik, A.; Inagaki, S. *J. Am. Chem. Soc.* **2001**, *123*, 691−696. (b) Mokaya, R. *Adv. Mater.* **2000**, *12*, 1681−1685.

(3) (a) Cavellec, M.; Riou, D.; Ferey, G. *Inorg. Chim. Acta* **1999**, *291*, 317−325. (b) Cavellec, M.; Riou, D.; Greneche, J. M.; Ferey, G. *Inorg. Chem.* **1997**, *36*, 2187−2190.

(4) (a) Barrer, R. M. *Zeolites* **1981**, *1*, 130−140. (b) Weller, M. T. *J. Chem. Soc., Dalton Trans.* **2000**, *23*, 4227−4240.

(5) (a) Wilson, S. T.; Lok, B. M.; Messina, C. A.; Cannan, T. R.; Flanigen, E. M. *J. Am. Chem. Soc.* **1982**, *104*, 1146−1147. (b) Cheetham, A. K.; Ferey, G.; Loiseau, T. *Angew. Chem., Int. Ed.* **1999**, *38*, 3269−3292.

(6) (a) Corbin, D. R.; Whitney, J. F.; Fultz, W. C.; Stucky, G. D.; Eddy, M. M.; Cheetham, A. K. *Inorg. Chem.* **1986**, *25*, 2279−2280. (b) Bu, X. H.; Feng, P. Y.; Stucky, G. D. *Science* **1997**, *278*, 2080−2085.

(7) (a) Brandão, P.; Valente, A.; Philippou, A.; Ferreira, A.; Anderson, M. W.; Rocha, J. *Eur. J. Inorg. Chem.* **2003**, *6*, 1175−1180. (b) Do, J.; Bontchev, R. P.; Jacobson, A. J. *J. Solid State Chem.* **2000**, *154*, 514−523.

(8) (a) Sun, D.; Cao, R.; Sun, Y.; Bi, W.; Hong, M. *Eur. J. Inorg. Chem.* **2003**, *7*, 1303−1305. (b) Chippindale, A. M.; Bond, A. D.; Law, A. D.; Cowley, A. R. *J. Solid State Chem.* **1998**, *136*, 227−232.

(9) (a) Zeng, Q. X.; Chen, L. S.; Li, Y. F.; Yang, G. Y.; Xu, J. Q. *Chem. J. Chin. Univ.* **2003**, *24*, 31−33. (b) Bontchev, R. P.; Iliev, M. N.; Dezaneti, L. M.; Jacobson, A. J. *Solid State Sci.* **2001**, *3*, 133−142.

(10) (a) Song, T.; Hursthouse, M. B.; Chen, J.; Xu, J.; Malik, K. M. A.; Jones, R. H.; Xu, R.; Thomas, J. M. *Adv. Mater.* **1994**, *6*, 679−680. (b) Chidambaram, D.; Natarajan, S. *Mater. Res. Bull.* **1998**, *33*, 1275−1281.

(11) (a) Neeraj, S.; Natarajan, S.; Rao, C. N. R. *Angew. Chem., Int. Ed. Engl.* **1999**, *38*, 3480−3483. (b) Natarajan, S.; Neeraj, S.; Rao, C. N. R. *Solid State Sci.* **2000**, 1, 87−98. (c) Chippindale, A. M.; Powell, A. V.; Jones, R. H.; Thomas, J. M.; Cheetham, A. K.; Huo, Q.; Xu, R. *Acta Crystallogr.* **1994**, *C50*, 1537−1540. (d) Venkatathri, N. *Indian J. Chem.* **2002**, *11*, 2223−2230.

(12) Meier, W. H.; Olson, D. H.; Baerlocher, Ch. *Atlas of Zeolite Framework Types;* Elsevier: London, 2001.

(13) (a) Yu. J.; Xu, R. *Acc. Chem. Res.* **2003**, *36*, 481−490. (b) Yu. J.; Xu, R.; Li, J. *Solid State Sci.* **2000**, *2*, 181−192.

(14) Yan, W.; Yu, J.; Shi, Z.; Xu, R. *Chem. Commun.* **2000**, *15*, 1431−1432.

(15) Wei, B.; Zhu, G.; Yu, J.; Qiu, S.; Xiao, F.; Terasaki, O. *Chem. Mater.* **1999**, *11*, 3417−3419.

(16) Yan, W.; Yu, J.; Xu, R.; Zhu, G.; Xiao, F.; Han, Y.; Sugiyama, K.; Terasaki, O. *Chem. Mater.* **2000**, *12*, 2517−2519.

(17) (a) Tédenac, J. C.; Vilminot, S.; Cot, L.; Norbert, A.; Maurin, M. *Mater. Res. Bull.* **1971**, *6*, 183−188. (b) Aléonard, S.; Gorius, M.-F. *C. R. Acad. Sci. Paris* **1989**, *309*, 683−687. (c) Srivastava, R. C.; Klooster, W. T.; Koetzle, T. F. *Acta Crystallogr.* **1999**, *B55*, 17−23. (d) Aléonard, S.; Le Fur, Y. *Mater. Res. Bull.* **1969**, *4*, 601−616.

10.1021/cm035316v CCC: $27.50
Published on Web 04/08/2004

To counter-balance the decreased negative charge, the construction of these fluoride-based analogues requires lower- charged metallic species such as M^{2+} and M^{+}. A prerequisite for materials to preserve the tetrahedral topology is to prevent the cation expansion to five or six; therefore metals with small cations such as lithium, beryllium, and boron are ideal candidates for fluoride-based frameworks.

Over the past few months we have reported new 1-D[19] and 2-D[20] tetrahedral based fluoride materials that have been synthesized using hydrothermal and slow evaporation ambient pressure techniques. The 1-D material, $[LiBe_2F_7][C_4N_2H_{12}][H_2O]_{1.5}$,[19] has a connectivity of two linked strands of $[BeF_4]$ and $[LiF_4]$ tetrahedra producing a corner-sharing "double" chain with each metal bonded through doubly bridging fluorides. The chains run parallel to each other and are encircled by doubly protonated piperazinium and solvent water molecules.

In addition we have synthesized 2-D sheet materials with two unique structural topologies.[20] The two materials can best be described as layers of $[BeF_4]$ and $[LiF_4]$ tetrahedra based around parallel rows of T4 and T3 "ladders". In both topologies terminal fluorides, bonded to just beryllium tetrahedra, lie in the interlayer spacing and hydrogen-bond to organo-amine templating species that line either side of the parallel arrangement of the sheets. The only difference in the two layers is that in one, triply bridging fluorides connecting two lithium centers align almost parallel to each other producing an −[Li−F−Li−F−Li]− linear chain, whereas in the other structure the same bridging groups lie almost perpendicular to each other forming a zigzag effect. Various organo-amine templating agents have been successfully employed in producing 2-D sheets such as ethylenediamine $[Li_2Be_2F_8][NH_2CH_2CH_2NH_2]$, methylamine $[Li_2Be_2F_8][CH_3NH_3]_2{\cdot}[H_2O]_2$, 3-methylbenzylamine $[LiBeF_4][C_6H_4(CH_3)CH_2NH_3]$, 4-chlorobenzylamine $[LiBeF_4][C_6H_4CH_2NH_3Cl]$, 1,3-diamminopropane $[LiBeF_4]_2[NH_3CH_2CH_2CH_2NH_3]$, and 3-phenyl-1-propylamine $[LiBeF_4][C_6H_5CH_2CH_2CH_2NH_3]$.

Construction of these 2-D structures indicates that the formation of 3-D materials might merely require the connection of the 2-D sheets together through the terminal fluorides that are currently involved in hydrogen bonding, and this could be achieved through an alteration of the geometry and charge on the organo-amine template. Here we report the compounds $[Li_2Be_2F_7][NH_4]$ **I** and $[Li_2Be_2F_7][CH_3NH_3]$ **II**, both organic templated framework lithiumberyllofluoro compounds containing a combination of T3 and T4 nets with small T6 channels containing the templating species. A material of the same components as compound **I** has been previously mentioned in the literature but no clear structural characterization was presented.[21] The analysis performed by Aleonard et al will be discussed in more detail later.

Experimental Details

Synthesis of $[Li_2Be_2F_7][NH_4]$, I. Ammonium fluoride (0.074 g, 0.2 mmol), beryllium fluoride (0.1 g, 0.2 mmol), 30% hydrofluoric acid (0.09 mL, 0.2 mmol), and lithium carbonate (0.015 g, 0.2 mmol) were dissolved in distilled water (1 mL) to give an overall molar ratio of 1:1:1:1 BeF_2/HF/Li_2CO_3/[A] where A = ammonium fluoride. The mixture was sealed in a 23-mL Teflon-lined Parr autoclave and heated at 180 °C for 24 h. After the mixture cooled, the title compound crystallized to form colorless block-type crystals that were recovered by filtration and air-dried. Yield 43% based on Be.

Synthesis of $[Li_2Be_2F_7][CH_3NH_3]$, II. Beryllium fluoride (0.1 g, 0.2 mmol), 30% hydrofluoric acid (0.17 mL, 0.4 mmol) and methylamine (0.25 mL, 0.2 mmol) were dissolved in distilled water (1 mL). The mixture was sealed in a Parr autoclave and heated at 150 °C for 2 h. After the mixture cooled, lithium carbonate (0.015 g, 0.2 mmol) was added to give an overall molar ratio of 1:2:1:1 for BeF_2/HF/Li_2CO_3/[A] where A = methylamine. (The two-stage process was used to aid the dissolution of BeF_2). The mixture was again sealed and heated at 150 °C for 24 h. After the mixture cooled, the title compound crystallized to form colorless rod-type crystals that were recovered by filtration and air-dried; yield 52% based on Be.

Caution. Toxicity of beryllium is a chronic problem. Appropriate precautions should be taken while handling and disposing of all beryllium-containing materials.

X-ray Crystallography. The crystal structure was determined from single-crystal X-ray diffraction (XRD) data. Single crystals of both **I** and **II** were mounted on the top of glass fibers and data were collected on a Nonius Kappa CCD area detector diffractometer using Mo Kα radiation ($\lambda = 0.71073$ Å); with ω and ϕ scans to fill the Ewald sphere at 298(2) K (and 120(2) K for the low-temperature structure). Absorption corrections were performed using SORTAV,[22] and the structures were solved by direct methods using SHELXS-97,[23] and structure refinement was by least-squares method SHELXL-97.[23] All the calculations were performed using the WINGX[24] system (Ver 1.64.05). The crystallographic data and detailed structure refinement information are shown in Table 1.

Polycrystalline samples of both **I** and **II** were ground using an agate pestle and mortar, and powder data were collected using both a Siemens D5000 and a Bruker D8/C2 diffractometer, using general area detector diffraction system (GADDS), (both Cu $K\alpha_1$ radiation; $\lambda = 1.54056$ Å) for preliminary phase identification. The results were compared to the simulated powder pattern from the single-crystal data to assess phase purity.

High-temperature powder XRD studies were undertaken to ascertain the structure of variable temperature phases for compound **I**. The data were collected using an Anton Parr HTK (high-temperature camera), 1200 high-temperature stage, attachment on a Bruker D8 Advance (Cu $K_{\alpha 1}$ radiation; $\lambda =$ 1.54056 Å) diffractometer. Powder data were collected at temperature values of 30, 200, 300, 350, 400, 350, 300, 200, and finally 30 °C; each pattern was collected for 60 min.

Neutron Diffraction. Medium-resolution neutron diffraction data for **I** (hydrogenous form) were collected at room temperature on the POLARIS instrument at ISIS, Rutherford Appleton Laboratories, over a period of approximately 4 h. The structure was refined using the Rietveld analysis program

(18) (a) Le Roy, J.; Aléonard, S. *Acta Crystallogr.* **1972**, *B28*, 1383−1387. (b) Chung, S. J.; Hahn, Th. *Mater. Res. Bull.* **1972**, *7*, 1209−1218. (c) Le Roy, J.; Aléonard, S. *Mater. Res. Bull.* **1970**, *5*, 409−418. (d) Anderson, M. R.; Brown, I. D.; Vilminot, S. *Acta Crystallogr.* **1973**, *B29*, 2625−2627. (e) Burns, J. H.; Gordon, E. K. *Acta Crystallogr.* **1966**, *20*, 135−138. (f) Collins, D. M.; Mahar, M. C.; Whitehurst, F. W. *Acta Crystallogr.* **1983**, *B39*, 303−306.

(19) Gerrard, L. A.; Weller, M. T. *Chem. Commun.* **2003**, *6*, 716−717.

(20) (a) Gerrard, L. A.; Weller, M. T. *J. Chem. Soc., Dalton Trans.* **2002**, *23*, 4402−4406. (b) Gerrard, L. A.; Weller, M. T. *Chem. Eur. J.* **2003**, *9*, 2−8.

(21) Le Roy, L.; Pontonnier, L.; Aléonard, S. *Mat. Res. Bull.* **1971**, *6*, 267−274.

(22) (a) Blessing, R. H. *Acta Crystallogr.* **1995**, *A51*, 33−37. (b) Blessing, R. H. *J. Appl. Crystallogr.* **1997**, *30*, 421−426.

(23) Sheldrick, G. M. SHELX-97 [Includes SHELXS97, SHELXL97], *Programs for Crystal Structure Analysis* (Release 97-2). University of Göttingen, Göttingen, Germany, 1997.

(24) Farrugia, L. J. WINGX. *J. Appl. Crystallogr.* **1999**, *32*, 837−838.

Table 1. Selected Crystallographic Data and Refinement Details of Single Crystal X-ray and Neutron for $[Li_2Be_2F_7][NH_4]$ I at Both Low and Room Temperature and Single Crystal X-ray Data at Low Temperature for $[Li_2Be_2F_7][CH_3NH_3]$ II[a]

	$Li_2Be_2F_7NH_4$ SXRD room temp	$Li_2Be_2F_7NH_4$ SXRD low temp	$Li_2Be_2F_7NH_4$ neutron room temp	$Li_2Be_2F_7CH_6N$ SXRD low temp
fw	182.94	182.94	183.04	196.97
space group	*Pnma*	$P2_1ca$	*Pnma*	*Cmcm*
Z	4	8	4	4
T, K	273(2)	120(2)	273(2)	120(2)
a, Å	10.024(2)	10.025(2)	10.0450(4)	6.9760(2)
b, Å	12.288(3)	12.221(2)	12.3370(5)	8.1020(3)
c, Å	4.9371(7)	9.842(2)	4.9321(2)	12.7442(5)
V, Å^3	608.1(2)	1205.8(4)	611.21(4)	720.30(4)
μ, mm^{-1}	0.260	0.262	N/A	0.226
D_x, mg m^{-3}	1.998	2.016	N/A	1.816
R1 [$I > 2\sigma(I)$]	0.0463	0.0408	N/A	0.0240
wR2 [$I > 2\sigma(I)$]	0.0819	0.0836	N/A	0.0610
data/restraints/parameters	688/6/65	2702/21/242	2871/0/76	465/0/41
R_F^2	N/A	N/A	0.071	N/A
χ^2	N/A	N/A	3.824	N/A

[a] Please note that the data for the low temperature were solved in the standard setting of $Pca2_1$ but for the purposes of comparison with the room-temperature cell the nonstandard setting of $P2_1ca$ is used.

Table 2. Important Bond Lengths (Å) for $[Li_2Be_2F_7][NH_4]$ I and $[Li_2Be_2F_7][CH_3NH_3]$ II (Estimated SDs Are Given in Parentheses)[a]

I	length Å	II	length Å
Li(1)−F(1)	1.815(6)	Li(1)−F(2)/F(2)^i	1.9053(17)
Li(1)−F(2)^1	1.856(6)	Li(1)−F(3)/F(3)^{iv}	1.8131(12)
Li(1)−F(2)^4	1.866(6)		
Li(1)−F(3)^3	1.839(6)		
Be(1)−F(1)	1.517(5)	Be(1)−F(1)	1.5867(17)
Be(1)−F(2)	1.545(5)	Be(1)−F(2)	1.5566(18)
Be(1)−F(3)	1.518(5)	Be(1)−F(3)^{ii}/F(3)^v	1.5280(11)
Be(1)−F(4)	1.574(5)		
Li(1)−Li(1)^5	3.156(7)	Li(1)−Li(1)^i	2.730(4)

[a] Symmetry transformations used to generate equivalent atoms: (*i*) $-x, -y, -z + 1$; (*ii*) $-x + 1/2, -y + 1/2, -z + 1$; (*iv*) $x, -y, -z + 1$; (*v*) $x - 1/2, -y - 1/2, -z + 1$; (1) $-x, -y, -z + 2$; (3) $-x, -y, -z + 1$; (4) $x + 1/2, y, -z + 3/2$; (5) $-x + 1/2, -y, z + 1/2$.

Table 3. Important Bond Angles (°) for $[Li_2Be_2F_7][NH_4]$ I and $[Li_2Be_2F_7][CH_3NH_3]$ II (Estimated SDs Are Given in Parentheses)[a]

I	angle °	II	angle °
F(1)−Li(1)−F(2)^1	110.6(3)	F(2)−Li(1)−F(2)^i	88.48(10)
F(1)−Li(1)−F(2)^4	104.7(3)	F(2)−Li(1)−F(3)^{iv}	104.58(4)
F(1)−Li(1)−F(3)^3	122.0(3)	F(2)^i−Li(1)−F(3)	104.58(4)
F(2)^1−Li(1)−F(2)^4	108.2(3)	F(2)−Li(1)−F(3)	114.92(4)
F(2)^1−Li(1)−F(3)^3	106.5(3)	F(2)^i−Li(1)−F(3)^{iv}	114.92(4)
F(2)^4−Li(1)−F(3)^3	104.1(3)	F(3)−Li(1)−F(3)^{iv}	123.97(13)
F(1)−Be(1)−F(2)	109.9(3)	F(1)−Be(1)−F(2)	105.43(11)
F(1)−Be(1)−F(3)	111.6(3)	F(1)−Be(1)−F(3)^{ii}	108.68(8)
F(1)−Be(1)−F(4)	108.4(3)	F(1)−Be(1)−F(3)^v	108.68(8)
F(2)−Be(1)−F(3)	110.5(3)	F(2)−Be(1)−F(3)^{ii}	110.58(8)
F(2)−Be(1)−F(4)	107.2(3)	F(2)−Be(1)−F(3)^v	110.58(8)
F(3)−Be(1)−F(4)	109.0(3)	F(3)^{ii}−Be(1)−F(3)^v	112.61(11)

[a] Symmetry transformations used to generate equivalent atoms: (*i*) $-x, -y, -z + 1$; (*ii*) $-x + 1/2, -y + 1/2, -z + 1$; (*iv*) $x, -y, -z + 1$; (*v*) $x - 1/2, -y - 1/2, -z + 1$; (1) $-x, -y, -z + 2$; (3) $-x, -y, -z + 1$; (4) $x + 1/2, y, -z + 3/2$.

GSAS[25] and the backscattering bank was used for the structure analysis. The scattering lengths in the refinement, including that for lithium, were standard values with the GSAS suite.

Fourier Transform Infrared Spectroscopy. FTIR spectra were collected using a Perkin-Elmer Spectrum One FTIR Spectrometer using KBr disks. Small samples of **I** and **II** were ground using an agate pestle and mortar to which dry KBr was added and re-ground. The mix was pressed into a disk and measured using the Spectrum software (v3.02).

Thermal Analysis. Thermogravametric and differential thermal analyses (TGA/DTA) were performed on samples of both **I** and **II** from 25 to 450 °C under static air conditions using a Polymer Laboratories PL-STA. Amounts of 8.46 mg for **I** and 5.56 mg **II** were used and heated at a rate of 10 °C/min. Powder data were collected of the residues from TGA analysis using the Bruker D8/C2 diffractometer.

Elemental Analysis. Microanalyses on carbon, hydrogen, and nitrogen, for both samples (**I** and **II**) were performed by MEDAC LTD using combustion analysis on CE-440 and Carlo Erba elemental analyzers.

Results and Discussion

The 3-D framework structure of compound **I**, as solved for the 298 K data, shows that the structure can be described as being constructed from the same underlying sheet topology as some 2-D $LiBeF_4$ layered materials previously synthesized.[20] As in the sheet material, each $[LiF_4]$ moiety bonds to two $[BeF_4]$ units through doubly bridged fluorides and links to two $[BeF_4]$ and two other $[LiF_4]$ units each through a triply shared vertex at F(2). Each $[BeF_4]$ unit vertex shares with four $[LiF_4]$ tetrahedra through two doubly bridged and one triply bridged fluoride leaving the final fluoride anion, which

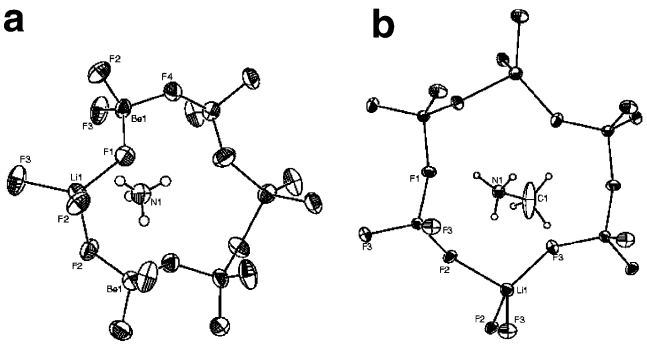

Figure 1. (a) Local coordination geometry of the inorganic $[Li_2Be_2F_7]^-$ framework of compound **I** showing the six-membered ring surrounding the ammonium NH_4 template. (b) Coordination geometry of the inorganic $[Li_2Be_2F_7]^-$ framework of compound **II** showing the analogous six-membered ring surrounding the CH_3NH_3 template. Ellipsoids shown are at the 40% probability level.

(25) Larson, A. C.; Von Dreele, R. B. GSAS *General Structure Analysis System;* LAUR 86-748; Los Alamos National Laboratory: Los Alamos, NM, 1986.

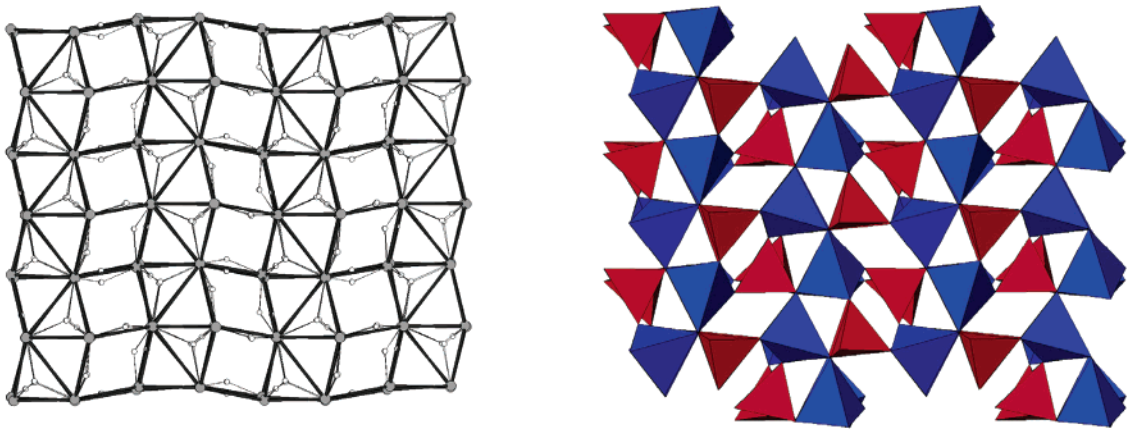

Figure 2. Diagrams showing the 2-D layer topology, of compound **I** viewed down *b*, within the 3-D network. Left figure shows metal-fluoride (light thin lines) and hypothetical metal−metal (dark thick lines) linkages, Li/Be (large spheres) and F (small spheres). Right-hand figure shows the vertical, zigzag "layers" of Li- (blue) and beryllium- (red) containing polyhedra.

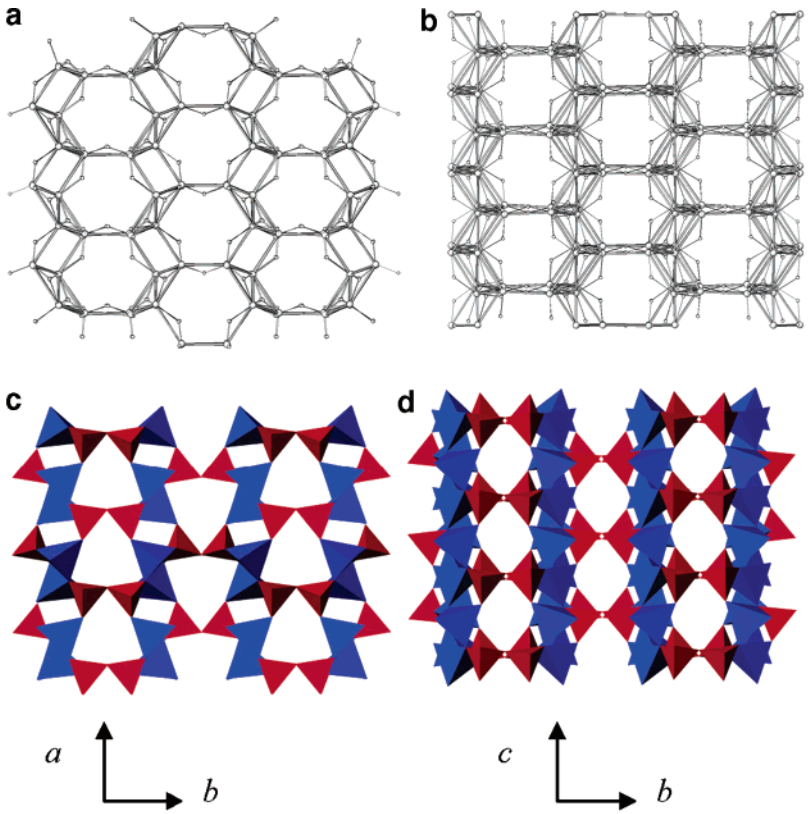

Figure 3. Schematic (T−F−T and T−T connectivity) and polyhedral representations of the 3-D network of **I**; no pore species are shown for clarification. (a) Ball and stick diagram of compound **I** viewed down the *a* axis showing the six-membered ringed channels. (b) Polyhedral packing diagram of Figure 3(a), same view. (c) Ball and stick diagram of compound **I** viewed down the *c* axis showing the six-membered ringed channels. (d) Polyhedral packing diagram of Figure 3(c), same view. LiF_4, blue tetrahedra; BeF_4, red tetrahedra in plots (b) and (d).

was terminal in the compound[20] but is now doubly bridged, linked to another [BeF_4] tetrahedra in an adjacent sheet. The Be−F bond lengths range from 1.518(5) to 1.574(5) Å with the F−Be−F angles varying from 107.2(3) to 111.6(3)°. The longer Li−F bond lengths occur over the range 1.815(6)−1.866(6) Å with the F−Li−F angles again slightly distorted from tetrahedral, with values between 104.1(3) and 122.0(3)°. These are again in good agreement with geometries for this type of species described previously in the literature,[17] Tables 2 and 3, and Figure 1(a).

The connectivity of the sheet extends parallel to the *ac* plane. This can be illustrated as infinite columns of T4 nets interspersed on either side with infinite columns of T3 nets, these run parallel to the *c* axis; a slice is shown schematically in Figure 2 where the bolder black lines show the metal−metal linkages through the bridging fluorides.

It can be seen that the two different metals form zigzag lines, within the 3-D framework, forming both edge sharing 3- and 4-nets. Similar fragments of this type have been observed in both *β*-beryllium oxide[26] and in aluminophosphate sheets.[27]

If viewed down the *c* axis the sheets can be best described as "ladder" chains of both T4 and T3 nets arranged in a −[4−3−3−4−3−3−4]− motif, running

parallel to the *a* axis as shown in Figure 3(a) and in a polyhedral view in 3(c).

The layers pack in an ABABA sequence; because of the zigzag nature of the sheets the beryllium centers, at opposing "maxima", are close together and the lithium cations are further apart. Adjacent beryllium atoms are linked together through doubly bridging fluorides (terminal fluorides in the 2-D sheet compounds of ref 20) that run parallel to the *b* axis and form six-membered nets.

These hexagonal nets, formed through two [LiF_4] and four [BeF_4] tetrahedra, are composed of 12 atoms—six metallic species and six bridging (two triply and four doubly) fluoride species. Three doubly bridging fluorides point into the pore, and the other three (two triply bridging fluorides and the "linking Be−F−Be" doubly bridged fluoride) pointing away. Neighboring linkages running parallel to the *a* axis form columns of the T6 nets. Adjacent columns are inverted with the nets aligned in the opposite direction. The T6 nets directly stack on top of each other forming infinite channels that run parallel to the *c* axis.

Perpendicular to the regular pattern of hexagonal T6 nets aligned with ladders of T3 and T4 rings lies another six-membered net that also forms parallel channels running along the *a* axis, Figure 3(b) and a polyhedral view in 3(d). Again, the "pore" is compiled of two [LiF_4] and four [BeF_4] tetrahedra, in total 12 atoms. The linking fluorides are composed of four doubly bridging and two triply bridging species. Again, three doubly bridging fluorides point into the pore and the other three (two triply bridging fluorides and one doubly bridged fluoride) point away.

Within the pore lies the amine templating species of an ammonium cation, which hydrogen bonds to the fluorides that point into the pore of the inorganic framework. Each ammonium cation is involved with seven hydrogen bonds through the four hydrogen atoms; these include two normal hydrogen bonds, from symmetry related H(2) atoms, one bifurcated (H(1)) and finally one trifurcated (H(3)). The lengths of the relatively weak hydrogen bonds range from 2.934(5) to 3.124(5) Å, (N−H···F) and are shown in Table 4. Note that the hydrogen atoms were fixed at a distance of ∼0.89 Å from the nitrogen atom. Figure 4(a) shows the H-bonding arrangement of the ammonium cation with the framework fluoride ions.

Two slightly different structures have been determined for this compound; first, a room temperature (273 K) data collection was solved giving the structure described above. A second data collection, at low temperature (120 K) on the same crystal showed a doubling of the unit cell in conjunction with a loss in symmetry. This loss in symmetry, therefore change (disorder), is attributed to the pore hydrogen species having a lesser motion at low temperature. At higher temperatures, the greater motion of the hydrogen atoms projects a larger disorder of the ammonium species in the pore, producing a cell with higher symmetry, from $Pnma$ to $Pca2_1$ (for the low T equivalent). The differences in crystallographic terms can be seen in Figure 4(a) and (b) and Table 1.

Table 4. Hydrogen Bonds for Compounds I and II [Å and °][a]

D−H···A	*d*(D−H)	*d*(H···A)	*d*(D···A)	⟨(*DHA*)⟩
N(1)−H(1)···F(1)	0.89(2)	2.32(2)	2.934(5)	126(2)
N(1)−H(1)···F(1)[7]	0.89(2)	2.32(2)	2.934(5)	126(2)
N(1)−H(2)···F(3)[8]	0.88(2)	2.30(3)	3.021(4)	139(3)
N(1)−H(3)···F(4)[9]	0.87(2)	2.33(4)	3.046(5)	139(4)
N(1)−H(3)···F(3)[10]	0.87(2)	2.58(3)	3.124(5)	122(3)
N(1)−H(3)···F(3)[4]	0.87(2)	2.58(3)	3.124(5)	122(3)
N(1)−H(1A)···F(3)	0.89(2)	2.14(2)	2.9080(6)	144.4(2)
N(1)−H(1B)···F(3)[vi]	0.89(2)	2.08(2)	2.9080(6)	155.3(2)
N(1)−H(1B)···F(2)[i]	0.89(2)	2.53(3)	3.0330(13)	116.2(2)
N(1)−H(1C)···F(2)[vii]	0.89(2)	2.24(2)	3.0330(13)	147.9(3)
N(1)−H(1C)···F(3)[viii]	0.89(2)	2.35(3)	2.9080(6)	121.2(2)

[a] Symmetry transformations used to generate equivalent atoms: (*i*) $-x, -y, -z+1$; (*vi*) $-x, y, z$; (*vii*) $-x, -y, z+1/2$; (*viii*) $-x, y, -z+3/2$; (4) $x+1/2, y, -z+3/2$; (7) $x, -y+1/2, z$; (8) $x, y, z+1$; (9) $x+1/2, y, -z+5/2$; (10) $x+1/2, -y+1/2, -z+3/2$.

The single-crystal analysis of compound **II** shows a 3-D framework topology slightly different from that of **I** but very closely related in both the inorganic stoichiometry and the basis of 3-, 4-, and 6T nets. The structure can also be described as a 2-D sheet linked together to adjacent symmetry related layers through Be−F−Be motifs. The sheets undulate, as observed in **I** (as well as the 2-D sheet materials of ref 20), again with the beryllium atoms lying at the peaks and troughs.

The Be−F bond lengths range from 1.528(1) to 1.587-(2) Å with the F−Be−F angles varying from 105.4(1) to 112.6(1)°. The longer Li−F bond lengths occur over the range 1.813(1)−1.891(2) Å with the F−Li−F angles strongly distorted from tetrahedral, with values between 88.5(1) and 124.0(1)°. These are again in good agreement with geometries for this type of species described previously in the literature,[17] Tables 2 and 3, and Figure 1(b).

The 2-D sheets in **II**, lying parallel to the *ab* plane, are constructed of [BeF_4] and [LiF_4] tetrahedral units. Each beryllium fluoride tetrahedra links four lithium, through two doubly and one triply bridging fluoride, and one beryllium center, through a doubly bridging species. The [LiF_4] building block connects four [BeF_4] units, through two doubly and two triply bridged fluoride species, and to a single [LiF_4] unit through two triply bridging fluorides. The connectivity between the two adjacent [LiF_4] tetrahedra forms an edge-sharing species that is unique in these materials but has been observed in transition metal zinco-phosphate based compounds.[28]

If metal−metal linkages are viewed, as in Figure 5, then the sheet displays ladders of edge-sharing 4-nets that run diagonally through the *ab* plane interspersed with parallel edge-sharing chains of both 3- and 4-nets that alternate in a ···[−4, 3, 3, 4−]··· sequence.

If viewed down the *a* axis, perpendicular to the sheet, the formation of corner-sharing 4-nets, linked through [LiF_4] units, extend parallel to the *b* axis. These columns link to adjacent, symmetry-related, chains through the doubly bridging fluoride atoms that extend perpendicu-

(26) Wells, A. F. *Philos. Trans. R. Soc. London* **1986**, *A319*, 291−335.

(27) (a) Williams, I. D.; Gao, Q.; Chen, J.; Ngai, L.; Lin, Z.; Xu, R. *Chem. Commun.* **1996**, *15*, 1781−1782. (b) Williams, I. D.; Gao, Q.; Chen, J.; Yu, J.; Xu, R. *Chem. Commun.* **1997**, *14*, 1273−1274.

(28) Chavez, A. V.; Nenoff, T. M.; Hannooman, L.; Harrison, W. T. A. *J. Solid State Chem.* **1999**, *147*, 584−591.

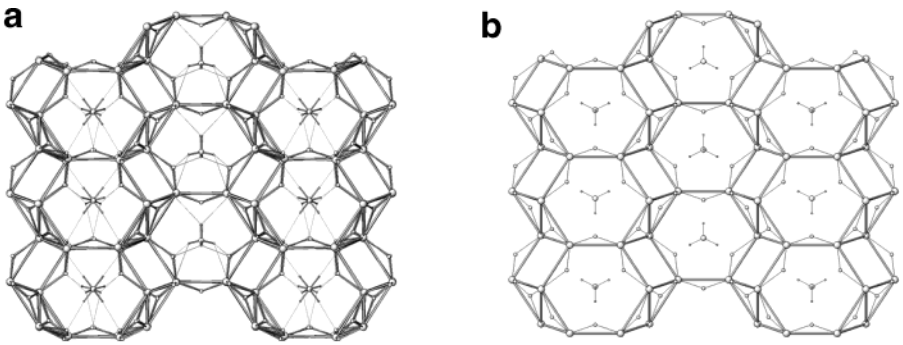

Figure 4. Schematic diagram showing the hydrogen bonding arrangement of the ammonium cation within the 6-MR channels for the room temp (left) and the low temp (right), viewed down the *a* and *c* axes, respectively. Hydrogen bonding shown as dashed lines.

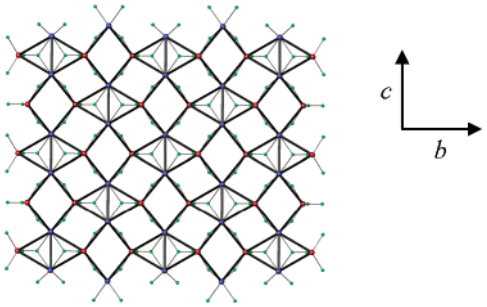

Figure 5. Schematic diagram showing the 2-D layer topology viewed down the *c* axis, of compound **II**, within the 3-D network, through both metal−fluoride (light thin lines) and hypothetical metal−metal (dark thick lines) linkages: Li, blue spheres; Be, red spheres; and F, small green spheres.

lar to the sheet in an AAAAA packing arrangement (Figure 6(a) and (d)). Two adjacent linking fluoride species connect together two sheets producing 6T net species that are composed of six metallic (four Be and two Li) and six linking fluoride species of which five point into the ring and one points into the next adjacent net.

A 45 ° rotation about the *c* axis gives a second set of six-membered hexagonal 6T nets, linked through the same bridging fluoride, but the 2-D sheet is best described as a ladder of 4 and 3T nets with a −[4, 3, 3, 4]− connectivity. The 6T rings pack either side of the 2-D sheet in an ABABA topology (Figure 6(b) and (e)). Finally, a second rotation of 45 ° through *c* gives a 3rd set of six- membered metallofluoro rings. This view, down the *b* axis, shows a parallel column arrangement of the nets linked through the edge-sharing [LiF_4] tetrahedra. The packing array is again in an AAAAA motif (Figure 6(c) and (f)).

In total three separate 6T net systems exist forming three unique channels running throughout the structure, Figure 6(a)−(d). Within the network of channels lies the organic templating agent of protonated methylamine, CH_3NH_3, Figure 7.

The C−N bond of the organoamine lies parallel to the *b* axis with both atoms falling on special positions in the *c*-centered orthorhombic cell. This causes disorder of both the three C−H and N−H bonds producing four equivalent sets about the *b* axis. The hydrogen atoms are generated and fixed to ride upon the parent atom and again as before the protons hydrogen bond to framework fluoride ions. In turn the assignments of

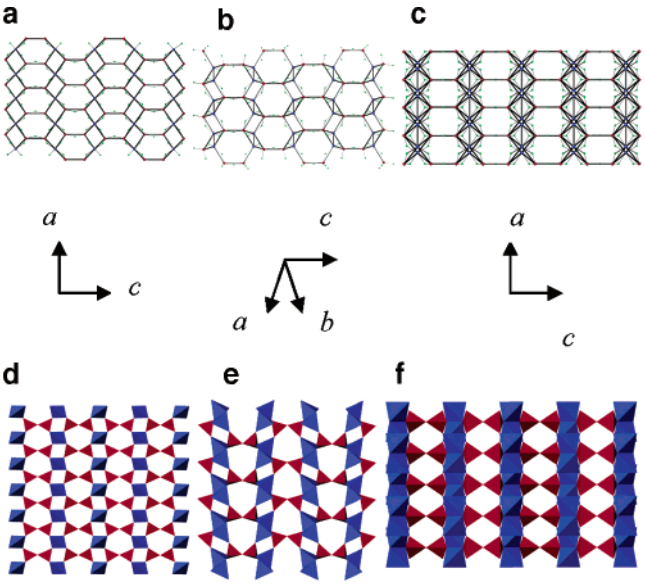

Figure 6. Schematic (T−F−T and T−T connectivity) and polyhedral representations of the 3-D network of **II**; no pore species are shown for clarification. (a) Ball and stick diagram of compound **II** viewed down the *a* axis showing the 1st set of six-membered ringed channels. (b) Polyhedral packing diagram of Figure 6(a), same view. (c) Ball and stick diagram of compound **II** viewed down the diagonal bisect of the *a* and *b* axes showing the 2nd set of six-membered ringed channels. (d) Polyhedral packing diagram of Figure 6(c), same view. (e) Ball and stick diagram of compound **II** viewed down the *b* axis showing the 3rd set of six-membered ringed channels. (f) Polyhedral packing diagram of Figure 3(e), same view. LiF_4, blue tetrahedra; BeF_4, red tetrahedra in plots (b), (d), and (f).

hydrogen bonds are somewhat tentative but in the range from 2.91 to 3.03 Å, as shown in Table 4.

Note. Further analysis, i.e., high-temperature powder X-ray and neutron analysis, was only available on compound **I**, as compound **II** was only ever produced in very small yields. Thermal gravametric and PXRD room-temperature data were recorded on the small amount of **II** available.

Thermal Properties. The thermal stabilities of compounds **I** and **II** were investigated using TGA/DTA in air between 25 and 450 °C. Compound **I** showed a total mass loss of 20.25%, that is assigned to a loss of both NH_3 (9.31%) and HF (10.94%), between 250 and 350 °C. DTA measurements exhibit two endothermal events, one at 320 °C and the second centered at 370 °C. The first event, due to the weight loss from the TGA, signifies the loss in ammonia and hydrogen fluoride−

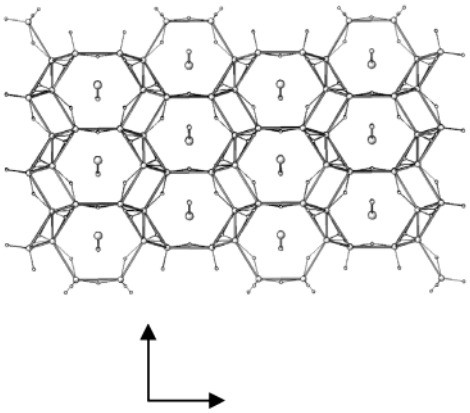

Figure 7. Schematic diagram showing the bonding arrangement of the methylammonium cation within the 6-MR channels, viewed down the diagonal bisect of the a and b axes, through both metal−fluoride (light thin lines) and hypothetical metal−metal (dark thick lines) linkages: Li/Be, large spheres; and F, small spheres in framework; C, large and N, small nonframework spheres.

at the same time as a major structural phase change. The second peak has no associated weight loss and is therefore a structural rearrangement. On cooling, further events occur due to crystallization exothermic events. The crystalline residue was analyzed further.

Compound **II** showed a total mass loss of 26.44% that is allocated to a loss of CH_3 (7.63% as CO_2 and H_2O), NH_3 (8.65%), and HF (10.16%), around 300 °C. The curve is very similar to that of compound **I** with DTA measurements exhibiting two endothermal events centered at 280 and 370 °C. The first thermal event, coincident with weight loss, assigned to carbon dioxide, water, ammonia, and hydrogen fluoride, produces a structural phase change. The second event has no associated weight loss but is assigned to a second phase change. On cooling, two clear exothermic thermal events occur (as in compound **I**) both due to crystallization of the material.

The resultant phases, from both TGA analyses, were identified through powder XRD methods using a Bruker C2 diffractometer. The TGA diagrams for compounds **I** and **II** are shown in Figure 8(a) and (b).

Powder X-ray Diffraction. Powder diffraction patterns were simulated using the model obtained from the single-crystal data. The patterns, compared against experimental, are provided as supplementary information Figures S1(a) and 1(b). The graph for compound **I**, run using the D5000 diffractometer, shows an excellent likeness of experimental to the theoretical pattern. Compound **II** also shows an excellent agreement to the simulated pattern. Powder data were collected of the residues from TGA analysis using the Bruker D8/C2 diffractometer to ascertain the nature of the thermal decomposition products. Diffraction patterns were taken for the two samples and analyzed using the JCPDS-ICDD database. For both compounds the residues were found to be a mixture of Li_2BeF_4 (major) and BeF_2 (minor). The results are summarized in the supplementary Figure S2 and support the evidence from the TGA that shows two separate exothermic crystallization events on the cooling curve.

In Situ Variable-Temperature Powder X-ray Diffraction. A variable-temperature powder XRD study was undertaken to ascertain what structural changes occur for compound **I** through the thermal events shown by the TGA/DTA data. Compound **I** was heated then cooled through the temperature regime of 30, 200, 300, 350, 400, 350, 300, 200, and 30 °C with a 60-min data collection at each temperature, and the results are shown in Figure 9.

The results show that as the temperature increases the peaks shift to a lower 2θ value indicating an increase in the unit cell dimensions.

At the first thermal event (300 °C), from TGA/DTA analysis, the PXD pattern has changed significantly and shows peaks that in turn can be assigned to Li_2BeF_4 and to $LiBeF_3$ (Figure S3); this would be stoichiometrically present after the loss of NH_3 and HF from compound **I**.

A further increase in temperature shows a gradual loss of peaks, signifying a decrease of crystallinity to an amorphous sample. Upon cooling, through the exothermic crystallization events, a main pattern emerges and is assigned to Li_2BeF_4; together with a small amount of BeF_2.

In conclusion, both compounds **I** and **II** undergo primary weight loss in the temperature range 25−400 °C due to oxidation of the templating species and the loss of the volatile gases of H_2O, CO_2, NH_3, and HF with a collapse of the framework to give a mixture of Li_2BeF_4 and $LiBeF_3$. The samples lose crystallinity at temperatures above 370 °C and leave an amorphous residue. Upon cooling to room temperature the thermodynamically stable product of Li_2BeF_4 crystallizes out as the major phase with a small amount of BeF_2, which indicates that two equivalents of $LiBeF_3$ (the high-temperature phase) recrystallize to give Li_2BeF_4 and BeF_2.

Neutron Diffraction. The starting model for the analysis of data from compound **I** was taken from the single-crystal refinement including possibly hydrogen positions. Initially the lattice parameters, background, and peak-shape profiles were refined to give a reasonable fit. The subsequent steps of refinement included varying the atomic positions and thermal parameters to give a good fit ($R_p = 1.57\%$, $R_{wp} = 1.23\%$, $Chi^2 = 3.83$) with only one non-hydrogen atom not refined anisotropically. Instability in the thermal displacement parameters for the three unique hydrogen atoms meant that these values were fixed at a U_{iso} value of 0.075 Å^2 but the atomic coordinates were fully refined and gave good agreement with the single crystal model but with a significantly smaller thermal displacement errors and thus, presumably, more accurate positions. Note that the extracted final profile fit factors are artificially low due to the good fitting of the high-intensity background profile in a hydrogenous material.

The final model shows a slight variation in the hydrogen positions leading to a greater distortion on the tetrahedral ammonium cation than observed in the single-crystal data (86.6(6)−132.7(7)° at 293 K compared to 103.5(5)−121.1(6)°). The N−H bond lengths are not fixed as in the single-crystal model and range from 0.838(21) to 1.004(14) Å, typical for N−H bond lengths. This gives rise to N−H···F hydrogen bonds of very similar length (2.934(5)−3.124(5) Å for single-crystal data and 2.943(5)−3.106(6) Å for neutron) although the

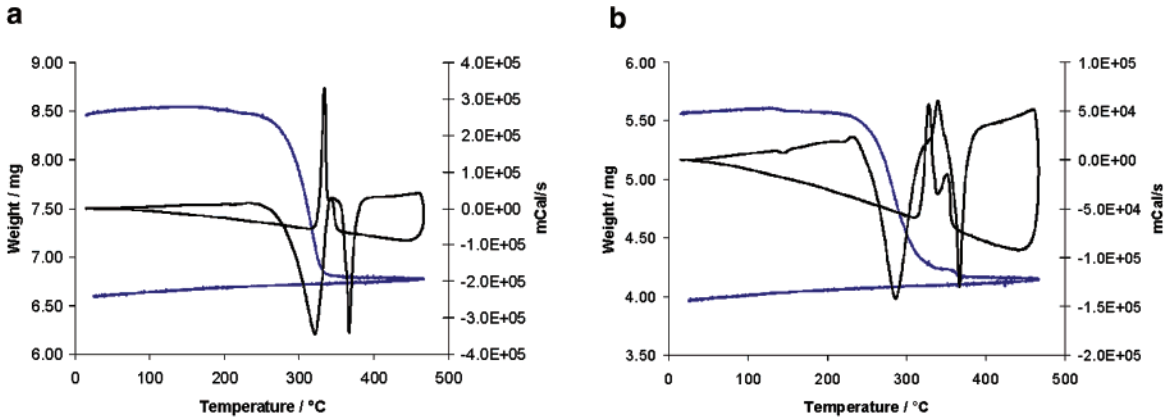

Figure 8. TGA plots of (a) compound **I** (left) and (b) compound **II** (right) showing both the (percentage) weight loss and DTA curve against temperature.

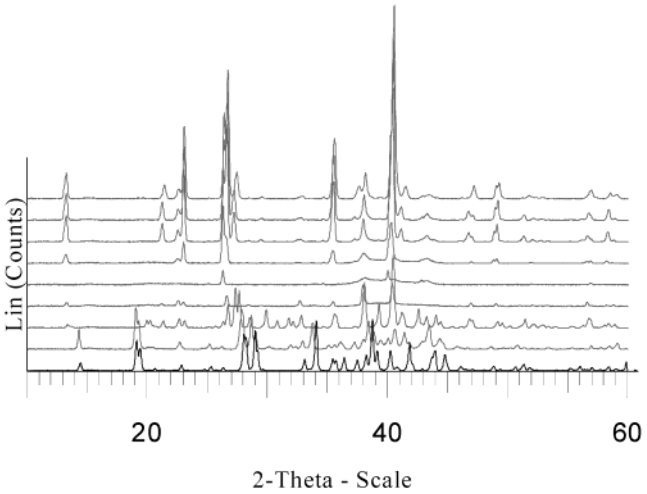

Figure 9. Plot of the powder diffraction patterns collected at selected temperatures using the in situ HTK device mounted on the D8 diffractometer: black, 30 °C; increasing temperatures 200, 300, 350, and 400 °C, followed by cooling to 350, 300, 200, and 30 °C are plotted sequentially and displaced vertically.

N−H···F angles encompass a wider range of values (117.4(9)−151.7(3)° for neutron compared with 122(3)−139(3)° for single crystal). These N−H···F hydrogen bonding values are typically of the same order that has been observed before in both the 1-D chain and 2-D sheet compounds.[18−20]

The hydrogen atoms of the ammonium compound and the fluorides of the framework are not favorably positioned for formation of very short linear hydrogen bonds resulting in the formation of the bifurcated and trifurcated hydrogen bonds. These types of weak interaction have also been observed in other amine-fluoride based materials such as lithium hydrazinium fluoroberyllate.[18]

The final atomic coordinate and thermal values are shown in Table 5. The fit is shown in Figure 10 and the powder CIF file is available in the Supporting Information.

Microanalysis. Microanalysis results for compounds **I** and **II** show very good agreement with theoretical data. Anal. Calc: Theoretical C, 0.00%; H, 2.20%; N 7.66%. Found: C, 0.12%; H, 2.39%; N, 7.83% for compound **I**. Anal. Calc: Theoretical C, 6.10%; H, 3.07%; N, 7.11%. Found: C, 5.99%; H, 3.24%; N, 6.93% for compound **II**.

Table 5. Atomic Coordinates for Compound I and Equivalent Temperature Factors (Å² × 10³)[a]

atom	*x*	*y*	*z*	U_{eq}/Å²
Be	−0.980(4)	0.1328(4)	0.714(1)	27(1)
	−0.997(2)	0.1309(2)	0.7193(5)	17.8(1)
Li	0.1519(6)	0.000(4)	0.795(1)	30(1)
	0.1478(7)	−0.005(1)	0.797(2)	24.4(1)
F1	0.447(2)	0.1189(2)	0.8102(5)	47(1)
	0.438(4)	0.1151(3)	0.8122(7)	21.0(1)
F2	−0.1897(2)	0.504(2)	0.8588(4)	35(1)
	−0.1904(4)	0.0457(4)	0.8550(7)	20.5(1)
F3	−0.1089(2)	0.1203(2)	0.4086(4)	45(1)
	−0.1150(4)	0.1214(4)	0.4087(9)	32.8(2)
F4	−0.1468(3)	0.2500	0.7955(5)	32(1)
	−0.1437(5)	0.2500	0.791(1)	17.1(2)
N	0.1377(5)	0.2500	0.1270(1)	38(1)
	0.1366(4)	0.2500	1.2665(9)	26.5(2)
H1	0.139(5)	0.2500	1.088(4)	57
	0.119(2)	0.2500	1.101(4)	75
H2	0.099(3)	0.187(2)	1.310(7)	57
	0.078(1)	0.194(1)	1.351(2)	75
H3	0.222(2)	0.2500	1.314(10)	57
	0.229(2)	0.2500	1.222(3)	75

[a] U(eq) is defined as one-third of the trace of the orthogonalized U^{ij} tensor (estimated SD in parentheses). First row − single-crystal data; and below − neutron data.

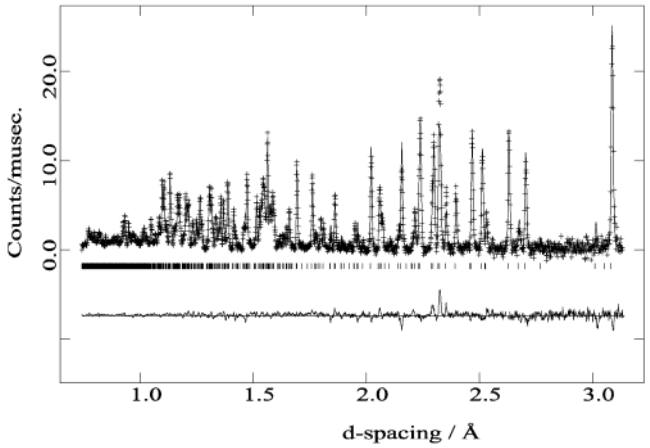

Figure 10. Neutron refinement profile of $[Li_2Be_2F_7][NH_4]$ run at room temperature on the Polaris instrument: crosses, observed data; upper continuous line, calculated data; lower continuous line, difference plot; and tick marks show the reflection positions.

Fourier Transform Infrared Spectroscopy. Present in the two spectra are four main broad bands at 495−860 cm^{-1}. These closely match with the known stretches of compound **I**,[29] and the peaks at 710 (for **I**)

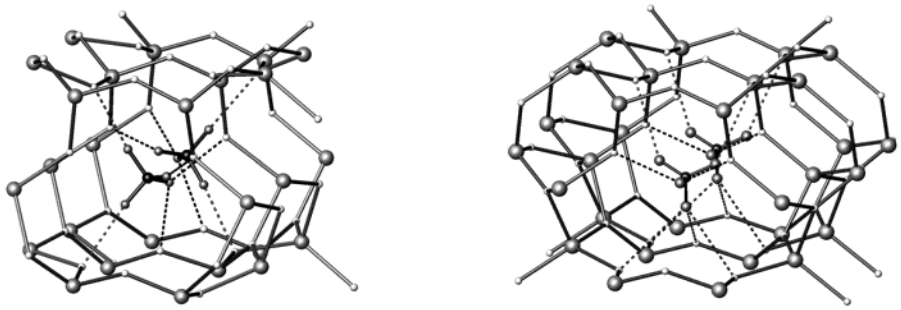

Figure 11. Hydrogen bonding arrangement of the ammonium cation within one of the 6-MR channels for the low temperature (left) and room temperature (right), viewed down the *a* and *c* axes, respectively. Ammonium ions are shown highlighted with hydrogen bonding as dashed lines.

and 733 (for **II**) are characteristic of the $Be_2F_7^{3-}$ grouping.[29] In comparison with orthofluoroberyllates (BeF_4^{2-}) there is only one band observed at this region around 800 cm^{-1}.

Slight differences occur at higher wavenumbers where compound **I** has a simpler region of bands at 3300 and 3104 cm^{-1} due to N−H stretching, whereas compound **II** has a more complicated region with both C−H stretching included at slightly lower wavenumbers (2967 and 2719 cm^{-1}). Both of these bands are very broad due to much hydrogen bonding in the system.[30] The spectra for compounds **I** and **II** are presented as Supporting Information.

Discussion

The two materials discussed in this paper have the same formula for the anionic part of the structure $[Li_2Be_2F_7]^-$ but form different structural topologies. The best way to differentiate the two compounds is to view the 2-D layers. In compound **I** columns of "regular" 4-nets are present, composed of two Be and two Li centers, which are decorated on either side by similar 4-net species that have been split into two 3-nets through the presence of a single triply bridging fluoride. In comparison, compound **II** displays a similar connectivity with columns of 4-net species that are compiled through the same bridging fluoride arrangement, but adjacent columns are formed through both the same 4-net species and a new "double" 3-net. As in compound **I**, triply bridging fluoride species transpose one 4-net into two 3-net species, but the 3-net species in **II** are formed though two triply bridging fluorides producing two LiF_4 tetrahedra sharing an edge.

The interconnection of these 2-D sheets is the same in both materials and both link through fluorides that reside perpendicular to the layers. This connection gives the apparent illusion, when viewed from certain directions, that the materials have the same connectivity via the formation of six-membered ring systems. This suggests that the organo-amine template plays an important role in determining the sheet topology but not the linkage of the sheets. This proposal must in fact be due to the weak interactions from the hydrogen bonding of ammonium and methylammonium cations when the inorganic framework is forming. The methylammonium cation has a less polar end (CH_3) that does not promote the formation of H-bonds and therefore could provide the explanation of the different sheets synthesized. Other larger amine templates have formed the 2-D sheet topology formed in compound **I**, but linking of the sheets becomes impossible due to the large inter-sheet distances forced upon the structure by the size of the structure-directing agents. So, using smaller organo-cationic species is required to form the 3-D frameworks.

Two single-crystal data sets were collected for compound **I**, one at room temperature and the other at a low temperature, to investigate the environments of the pore species. The main difference is in the relative orientation of the pore species. As the sample is cooled, a phase transition occurs as some ammonium groups adopt two fixed orientations in the pores and the framework undergoes small conformational changes in response to the modified hydrogen bonding pattern. At a higher temperature (298 K) the pore species presumably undergo large torsional motions and can oscillate between orientations, whereas at a lower temperature (120 K) the positions become fixed, therefore a loss in symmetry is observed for the lower temperature cell—from *Pnma* to *Pca*2(1). Figure 4(a) and (b) shows the two distinct environments with every other column of 6-nets housing the loss in symmetry (from an *a* glide to a 2_1 screw axis, viewed down the *c* axis). A more detailed representation of the changes in hydrogen bonding of the ammonium ion in the six ring channel is shown in Figure 11. In the low-temperature structure, alternate ammonium ions in half the six ring channels are oriented in different directions, whereas in the room temperature form all ammonium ions have the same orientation relative to the framework.

The literature states that the ammonium material, compound **I**, has been previously synthesized in 1971 by Aleonard.[21] The reported unit cell and space group match exactly with the room-temperature cell obtained in this paper, although no clear structural data were presented and the formula was incorrectly given as $Li_3NH_4(BeF_4)_2$. No other analysis was performed on these compounds in the previous paper. In a later paper, again by Aleonard,[29] a single crystal of a rubidium equivalent material was solved; the formula this time was found to be $RbLi_2Be_2F_7$ and not $Li_3Rb(BeF_4)_2$ as previously thought. Reference 21 also states that the other species with NH_4, Tl, and Cs (as countercation species) will be expected to have the same anionic structural topology.

(29) Vicat, P. J.; Tran Qui, D.; Aléonard, S. *Acta Crystallogr.* **1976**, *B32*, 1356−1362.

(30) Hamilton, W. C.; Ibers, J. A. *Hydrogen Bonding in Solids*; W. A. Benjamin: New York, 1968; p 284.

Compound **II** is the second 3-D lithiumberyllofluoro compound formed using a larger "than NH_4" amine templating species. It possesses a new 3-D tetrahedral framework structure unlike any other seen in other porous materials such as AlPOs. As with compound **I**, the 3-D architecture is composed of layers of 2-D sheets joined together (2-D materials have been synthesized in the group that adopt this topology); compound **II** might therefore have a 2-D analogue associated with it. However, attempts to synthesize a 3rd new 2-D layered material with the sheet topology have so far been unsuccessful.

In summary, this paper shows the first single crystal (at room and low temperature), powder X-ray, and neutron analysis of the compound $[Li_2Be_2F_7][NH_4]$ and reports a single-crystal analysis of a new material of stoichiometry $[Li_2Be_2F_7][CH_3NH_3]$. Both compounds display a 3-D inorganic fluoride-based framework that forms around the organo-amine templating species through hydrogen bonding interactions. The stability of the two structures is strongly dependent on the templating channel species. The collapse of the two frameworks is observed when the organo-amine molecules are removed (burned out) suggesting no porosity exists. The irreversibility of the materials proves the dependency of the N−H···F hydrogen bonding interactions from template to framework.

Recent exploratory hydrothermal reactions with lithium/beryllium/fluoride/amine media have afforded a number of new 1-D, 2-D, and 3-D materials. In these structures the fluoride ion can be shared by more than two tetrahedra, i.e., it is triply bridging which may be understood in terms of Pauling's electrostatic bond strengths: that is, in silicates and zeolites the valence of oxygen is satisfied by two Si^{4+} or $Si^{4+} + Al^{3+}$ but the lower charged fluoride ion requires two beryllium or one beryllium and two lithium ions to meet its bonding demands. The new architecture, of compound **II**, suggests that other templating species could be used to synthesize new topologies adding to the small known family of tetrahedral-based fluoride networks.

Acknowledgment. Financial support from the EPSRC (Grant GR/R12077), the use of the Kappa CCD diffractometer through Prof. M. B. Hursthouse, and MEDAC for the microanalysis results are gratefully acknowledged.

Supporting Information Available: X-ray crystallographic data in CIF format for compound **I** at room and low (120 K) temperatures and compound **II**. Infrared spectra of compounds **I** and **II** (pdf). Powder CIF from neutron data for compound **I**. This material is available free of charge via the Internet at http://pubs.acs.org.

CM035316V